Magnetic phase diagram of α-$NdIr_2Si_2$

M. Mihalik,[1,2,*] J. Pospíšil,[1] A. Hoser,[2] and V. Sechovský[1]
[1]*Charles University, Faculty of Mathematics and Physics, Department of Condensed Matter Physics, Ke Karlovu 5, CZ-12116 Prague 2, Czech Republic*
[2]*Helmholtz-Centre Berlin for Materials and Energy, Hahn Meitner Platz 1, D-14109 Berlin, Germany*
(Received 16 November 2010; revised manuscript received 3 March 2011; published 12 April 2011)

Magnetism in α-$NdIr_2Si_2$ single crystals has been probed through specific-heat, magnetization, magnetic susceptibility, and electrical resistivity measurements as a function of temperature, under an applied magnetic field, and for the magnetization curves under high hydrostatic pressures. Neutron diffraction experiments performed with powder and single-crystal samples were focused on microscopic aspects. Two collinear (Nd moments along the c axis) antiferromagnetic phases are found at low temperatures: a longitudinal sine-modulated structure with the magnetic propagation vector $\mathbf{k} = (0\ 0\ 5/6)$ at temperatures 18.2(2) K $< T <$ 32.3(3) K ($+T_N$) and a simple AF1-type structure; $\mathbf{k} = (0\ 0\ 1/2)$ for $T <$ 18.2(2) K ($+T_t$). Both of the magnetically ordered phases can be destabilized by applying a strong magnetic field along the c axis. The character of the unusual magnetic-field-induced phases is discussed, and the complex magnetic phase diagram is constructed. Applied hydrostatic pressure yields an increase of both T_N and T_t. The determined physical properties of α-$NdIr_2Si_2$ are discussed in the context of behavior of α-$PrIr_2Si_2$.

DOI: 10.1103/PhysRevB.83.134414 PACS number(s): 75.30.Kz, 75.47.Np, 65.40.−b, 72.15.Eb

I. INTRODUCTION

Since the discovery of polymorphism in the compound $LaIr_2Si_2$ by Braun *et al.*,[1] research into AB_2X_2 intermetallic compounds have attracted the attention of physicists. In addition to $LaIr_2Si_2$, polymorphism has been reported for $CeIr_2Si_2$,[2–4] $PrIr_2Si_2$,[5,6] $NdIr_2Si_2$,[7] and $YbIr_2Si_2$[8] as well as the related RNi_2As_2 (R = La, Ce, Pr, Nd, Sm) compounds.[9] In each case, polymorphism gives two phases: the α phase, which adopts the tetragonal $ThCr_2Si_2$-type crystal structure (space group $I4/mmm$), and the β phase, which adopts the tetragonal $CaBe_2Ge_2$-type structure (space group $P4/nmm$).[3,5,7] The β phase is the high-temperature phase, but it can be obtained at room temperature by rapid cooling from the melt or preparing single crystals by the flux method[8] or the Czochralski method.[4] The β phase is metastable at room temperature and can be transformed to the α phase by annealing the material at slightly elevated temperatures.[5] The α phase can be obtained at room temperature directly by sufficiently slow cooling from the melt.[10]

To date, magnetism in $NdIr_2Si_2$ has been studied only in the α phase[10] by measuring bulk powder magnetic susceptibility and neutron powder diffraction (NPD). According to this paper, the compound orders antiferromagnetically below T_N = 33(1) K with Nd moments locked along the c axis forming a simple AF1-type structure ($+-+-$ stacking along c). The susceptibility data reported in Welter *et al.*[10] show an unexplained anomaly at 18(2) K, which might be due to an additional magnetic phase transition. The lack of detailed experiments motivated us to prepare the single crystals of $NdIr_2Si_2$ in order to clarify the physics (preferably in both polymorphic phases).

In this paper we present information from the crystal growth experiments, the specific heat, magnetization, magnetic susceptibility, and electrical resistivity data for α-$NdIr_2Si_2$ single crystals at various temperatures in magnetic fields up to 14 T. Magnetization data were also collected with the crystal exerted to hydrostatic pressures. In order to understand the magnetic structure, neutron powder and single-crystal diffraction experiments were performed at low temperature and, in the case of the single crystal, in magnetic fields up to 6 T.

II. SAMPLE PREPARATION AND EXPERIMENTAL SETUP

A $NdIr_2Si_2$ single crystal was grown by the Czochralski method in a tri-arc furnace using a stoichiometric melt of Nd, Ir, and Si of purity of at least 3N. In the case of β-$NdIr_2Si_2$, a stoichiometric mixture of the starting elements was arc-melted in the furnace, and the power was abruptly switched off to let the sample cool down rapidly in the water-cooled copper crucible. However, this procedure did not provide the desired single β phase. Since α-$NdIr_2Si_2$ orders magnetically at T_N, and undergoes another phase transition at T_t,[10] it was decided that the bulk experiments on the two-phase material would not be performed. In the rest of the paper we deal only with the α-$NdIr_2Si_2$ phase.

Initial phase identification of the samples was done using x-ray powder diffraction (XRPD) measurements using the Cu Kα doublet x-ray line in the classical Bragg-Brentano geometry. Part of the single crystal was ground and examined by XRPD at room temperature. The Rietveld analysis of the powder pattern (Fig. 1) revealed two phases, α-$NdIr_2Si_2$ and β-$NdIr_2Si_2$, respectively, with refined lattice parameters in very good agreement with previously published data (Table I). To obtain the pure α phase, the crystal was annealed at 900 °C for 12 h. The XRPD check of the annealed samples has confirmed that the samples contain the single α phase. The lattice parameters of the two polymorphic phases determined by XRPD at room temperature gave nearly the same unit cell volume, whereas the c/a ratio differed by as much as 5%. The Laue pattern of the annealed rod proved that the material was a single crystal with large mozaicity of around 1°, which may be ascribed to the microcracks induced by the β- to α-$NdIr_2Si_2$ phase transition.

TABLE I. The lattice parameters of the both phases of $NdIr_2Si_2$.

	a (nm)	c (nm)	c/a	V (nm^3)	Reference
α phase	0.4080(2)	1.0082(5)	2.471	0.1679	This work
	0.4078	1.0097	2.48	0.1679	Ref. 7
β phase	0.4144(4)	0.9832(2)	2.373	0.1688	This work
	0.4144	0.9851	2.38	0.1692	Ref. 7

The NPD experiment was done on the E6 diffractometer at the BER-II reactor (Berlin) using a standard Orange cryostat and two position-sensitive 2D detectors. For this experiment a neutron wavelength of 2.44 Å was used. Whole pattern data were collected ($17^\circ < 2\theta < 107^\circ$) for temperatures 2, 7, 10, 15, 20, 25, and 40 K. Since iridium is a strong neutron absorber, a vanadium container with an inner diameter of 6 mm and an aluminum container with the inner diameter of 3.75 mm, respectively, were used as sample holders to correctly describe the absorption of the compound. We have included the absorption corrections in the Rietveld analysis of the powder pattern. This Rietveld analysis was done using the FULLPROF program.[11]

For the NPD experiments, approximately 5 g of a polycrystalline sample was synthesized by arc melting. The obtained material was annealed at 900°C for 12 h. After the annealing it was found that the sample contained two phases: the majority α-$NdIr_2Si_2$, and approximately 21% of the β phase as determined by XRPD, or 18% of the β phase as determined by NPD. Apparently, in the polycrystalline samples, the temperature for the β-to α-phase transition need to be higher than for the single-crystal samples. This may be caused by the presence of the grain boundaries in the polycrystalline sample, and subsequent pinning of the β phase to these boundaries (detailed classical theory can be found, for example, in Ref. 12).

The neutron single-crystal diffraction experiment was performed on the E1 triple-axis spectrometer in the BER-II reactor (Berlin). Two different experimental configurations were used in the experiments. In the first experimental configuration we used the standard Orange cryostat, a wavelength of 2.446 Å (PG monochromator), and performed *hkl* scans from (1 0 −0.1) to (1 0 4.05), from (2 0 −1) to (2 0 2), and from (0 0 2.7) to (0 0 3.1). In the second experimental configuration we used the horizontal HM1 magnet, applied a magnetic field along the *c* axis ±2°, and performed *hkl* scans from (1 0 −0.8) to (1 0 0.45). To allow the desired reflections to pass through the windows of the magnet, a wavelength of 1.240 Å (GE monochromator) was chosen. All scans were performed in the temperature range 1.7 K < T < 40 K.

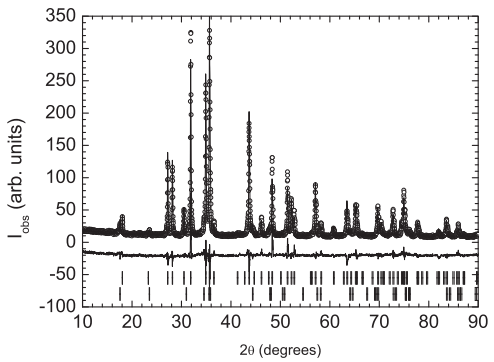

FIG. 1. The XRPD pattern of the as-grown sample (points) together with the Rietveld fit (line through points), difference between observed data and model (line below points), and peak positions of the β phase (upper set of peaks) and α phase (lower set of peaks).

Specific heat measurements were performed using the time relaxation method implemented in the Physical Property Measurement System (PPMS) from Quantum Design. For this experiment a disk sample aligned with the *c* axis parallel to the magnetic field with a mass of 12.36 mg was used. As the nonmagnetic analog sample needed for the comparative analysis of the specific heat, an α-$LaIr_2Si_2$ polycrystal was also prepared using a procedure described elsewhere.[4]

To measure magnetization with respect to magnetic field in fields of up to 14 T, we used the extraction magnetometer of the PPMS apparatus. A cube-shaped sample with a mass of 32.7 mg was prepared, where the cube edges were oriented parallel to the principal crystallographic axes. The same sample was used for the fine DC magnetization measurements performed in low magnetic fields in the squid magnetometer (magnetic property measurement system, MPMS from Quantum Design).

The hydrostatic pressure experiment was performed with the MPMS apparatus in combination with a clamped CuBe cell. The details of the cell can be found elsewhere.[13] For the experiment, we used Daphne oil as a transmitting medium and Pb as an internal pressure sensor. Based on the uncertainty in the measurement of the superconducting transition of Pb, we estimate that the determined pressures have an absolute error of 50 MPa. The pressure cell was clamped at room temperature. The different thermal expansion of CuBe cell, and the Daphne oil leads to increasing pressure exerted on the sample with increasing temperature: +10 MPa at $T = T_t$ and +20 MPa at $T = T_N$ compared with $T = 7.20$ K (temperature of the superconducting phase transition of lead in zero magnetic field, and ambient pressure[14]) which was taken into account in our data analysis. For the hydrostatic pressure experiment, we used the cubic sample with the *c* axis aligned parallel to the applied magnetic field.

Since the samples were very brittle, for the resistivity and magnetoresistivity measurements we had to use the bar-shaped samples with a typical length of 2 mm and a cross section of 0.6 mm^2. All measurements were performed using the four-probe AC method implemented in the PPMS apparatus.

III. EXPERIMENTAL RESULTS AND DISCUSSIOIN

A. Bulk measurements

The specific heat data (Fig. 2) exhibit two anomalies which confirm the existence of two phase transitions, associated with T_N, and T_t reported by Welter *et al.*[10] Both of the anomalies are shifted to lower temperatures when the magnetic field is applied along the *c* axis (Fig. 2), which implies that both the phase transitions are of magnetic origin. Using the comparative analysis of the specific heat with data measured

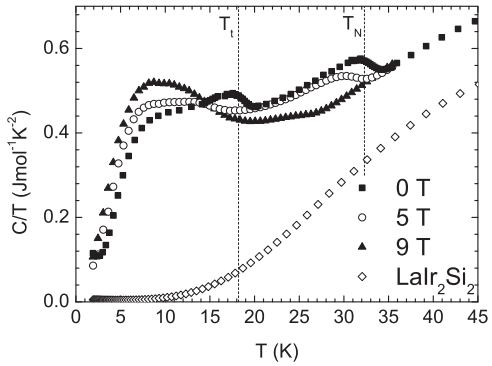

FIG. 2. The specific heat of α-$NdIr_2Si_2$ (C_p/T versus T plot) compared with the specific heat of polycrystalline α-$LaIr_2Si_2$. The magnetic field in this experiment was applied along the c axis.

for the nonmagnetic analog of single-phased α-$LaIr_2Si_2$ we calculated the magnetic entropy (Fig. 3) of α-$NdIr_2Si_2$. The magnetic entropy exhibits no clear feature at T_t, and T_N, respectively, only steps of the first temperature derivative of the entropy can be recognized (insert of Fig. 3). The increase of the magnetic entropy with respect to the applied magnetic field (Fig. 3) at temperatures below 40 K is ascribed to the shift of T_N, and T_t to lower temperatures.

The relatively broad anomalies in the specific heat at the magnetic phase transitions prevented us determining the values T_N, and T_t precisely. Therefore, we measured the DC susceptibility in a very low magnetic field of 0.1(+3; −1) mT with $B||c$ axis (Fig. 4). The zero-field-cooled (ZFC) data shows a kink at 18.2(2) K, and a maximum at 32.3(3) K, and is ascribed to the two anomalies to the magnetic phase transitions at T_N, and T_t, respectively. Surprisingly, the magnetization measured when cooling from the paramagnetic state in the same magnetic field exhibits a shift of T_t to 15.5(2) K. After this scan the magnetization during heating the sample was again measured. In the third scan our data fitted very well with the data obtained for the ZFC scan. The evolution of the hysteresis of the temperature dependence of the susceptibility near T_t were studied by scans performed at low magnetic fields of 10 to 50 mT and by the magnetization measurements up to $B = 2.5$ T with $B||c$ axis. These magnetization measurements show hysteresis of T_t in all applied magnetic

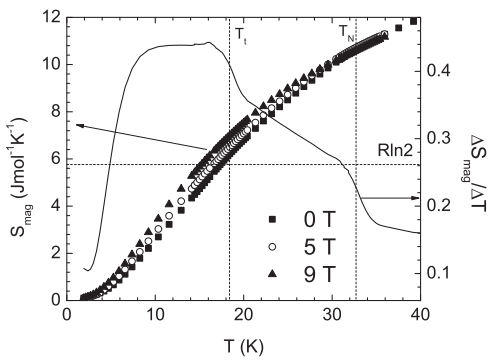

FIG. 3. The calculated magnetic entropy and the derivation of the entropy with respect to the temperature at magnetic field $B = 0$ T.

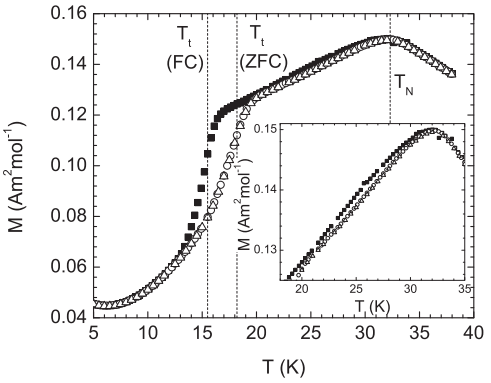

FIG. 4. The magnetization measured at set field of 0.1(+3;−1) mT with $B||c$ axis. The squares represent the data measured during cooling in magnetic field of 0.1(+3;−1) mT, the circles represent the data measured during heating after the previous cooling in magnetic field of 0.1(+ 3;−1) mT, and the triangles represent the data measured during heating after the previous cooling in a zero magnetic field. In the inset the detail of the graph for temperatures $T_t < T < T_N$ is plotted.

fields. Note that the magnetization of $NdIr_2Si_2$ measured during cooling is systematically higher at $T_t < T < T_N$ than the magnetization measured during heating (inset of Fig. 4).

The inverse susceptibility ($1/\chi$) calculated from DC magnetization data measured at 3 and 7 T for both the a and c crystallographic direction (Fig. 5) is linear with temperature in the range 60 K $< T <$ 300 K for the a axis and in the range 120 K $< T <$ 300 K for the c axis. In these temperature ranges we were able to fit the susceptibility with the Curie-Weiss law

$$\chi = \frac{C}{T - \theta_p} \tag{1}$$

$$C = \frac{N\mu_{\text{eff}}^2}{3k_B} \tag{2}$$

with coefficients $\theta_{p,a} = -61(1)$ K, $\mu_{\text{eff},a} = 3.83(3)\ \mu_B$ for the a axis and $\theta_{p,c} = 23.6(5)$ K, $\mu_{\text{eff},c} = 3.88(3)\ \mu_B$ for the c axis. The effective moment for both crystallographic directions is equal to the $\mu_{\text{eff,poly}} = 3.8(1)\ \mu_B$ reported for the polycrystalline sample[10] within the experimental error.

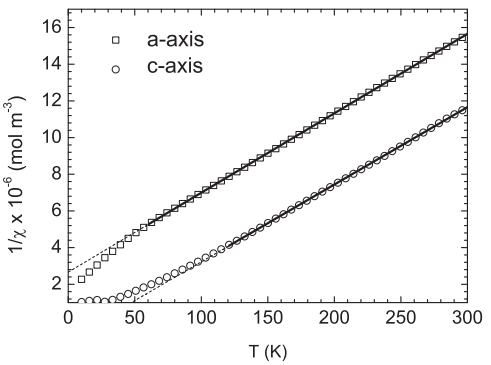

FIG. 5. The inverse susceptibility calculated from the magnetization data measured at 3 and 7 T along the main crystallographic axes.

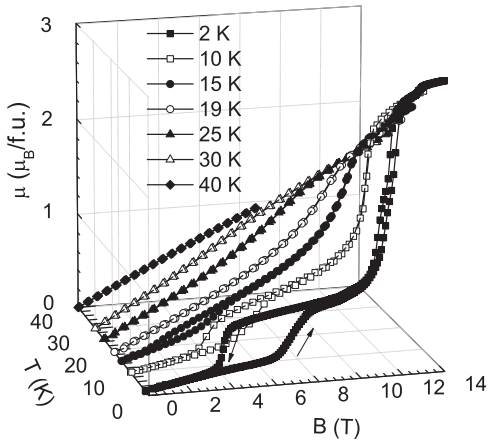

FIG. 6. The plot of selected magnetization curves for $B||c$ axis.

All these μ_{eff} values are, however, systematically higher than the theoretical value for the free Nd^{3+} ion (3.62 μ_B). Existence of an effective moment associated with the Ir ion of approximately 0.2 μ_B may explain this apparent discrepancy. No clear indication of an Ir magnetic moment, however, was obtained during the neutron diffraction experiments discussed in the following section. The large difference between the values of the paramagnetic Curie temperature $\theta_{p,a}$, and $\theta_{p,c}$ respectively, is due to the considerable magnetocrystalline anisotropy in the paramagnetic state being apparently the effect of the crystal field acting on the Nd^{3+} ions. Deviations from linearity of $1/\chi$ versus T plots at temperatures below 60 (120) K can be also ascribed to the crystal field interaction.

The strong magnetocrystalline anisotropy, which is a consequence of the crystal field in α-$NdIr_2Si_2$, can be demonstrated by the magnetization curves (Fig. 6): The magnetization curves measured with magnetic field (up to 9 T) parallel to the a axis, $M_a(B)$, are almost linear at temperatures up to 40 K. On the other hand, the magnetization curves measured with the magnetic field applied along the c axis [$M_c(B)$] exhibit two metamagnetic transitions (MT) for temperatures lower than T_t and one MT for temperatures $T_t < T < T_N$.

The first MT, which occurs at 2 K at a magnetic field of 6.8 T and has a hysteresis of 3.1 T, moves to lower fields, and the hysteresis becomes reduced with increasing temperature. This MT disappears at T_t. At $T = 2$ K the second MT occurs as a relatively sharp feature at 11.6 T with a small hysteresis of 0.3 T. It becomes gradually shifted to lower fields, and smeared out with increasing temperature, disappearing at temperatures around T_N.

The $M_c(B)$ curves are very similar to the $M_c(B)$ curves measured on the α-$PrIr_2Si_2$ isostructural analog.[6] The main difference between both compounds is that the MTs in α-$NdIr_2Si_2$ occur at slightly lower magnetic fields, and T_N and T_t are slightly lower than in case of α-$PrIr_2Si_2$. Consequently, one may expect that the hierarchy of magnetic interactions is the same in both compounds. Note that the lattice parameters of the $PrIr_2Si_2$ are less than 0.5% larger than in case of $NdIr_2Si_2$ (compare data from Ref. 5 and Table I), and the c/a ratio is practically the same for both compounds. From the de Gennes scaling

$$T_{\text{ord}} \approx [g\,(JLS) - 1]^2\, J\,(J+1)\,, \tag{3}$$

where $g(JLS)$ is the Landé g factor and J is the total angular momentum of the magnetic ion, we should expect the higher ordering temperature for α-$NdIr_2Si_2$ compared with α-$PrIr_2Si_2$, but we have observed the opposite. This suggests that the leading exchange interactions in α-$NdIr_2Si_2$ are probably slightly weaker than in case of α-$PrIr_2Si_2$.

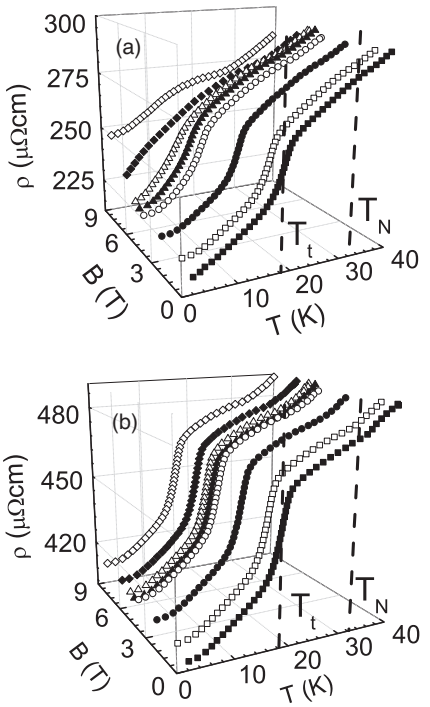

FIG. 7. The resistivity measured in the experimental configuration (a) I || a axis, $B||c$ axis and (b) $I||c$ axis, $B||a$ axis. The magnetic fields at which the data were taken are as follows: (solid squares) 0 T; (open squares) 1 T; (solid circles) 3 T; (open circles) 5 T; (solid triangles) 5.5 T; (open triangles) 6 T; (solid diamonds) 7 T; (open diamonds) 9 T.

The resistivity (ρ) measured along both main crystallographic axes decreases linearly with decreasing temperature in the temperature range 300–40 K, suggesting the metallic character of the compound. At lower temperatures than 40 K (Fig. 7) we observed two anomalies in the resistivity: a change of slope at T_N and a sudden drop below T_t. The fact that the c axis is the easy magnetization direction of the system can be demonstrated by the shifting of both anomalies to lower temperatures with applied magnetic field along the c axis [Fig. 7(a)] contrary to negligible response when the magnetic field applied along the a axis [Fig. 7(b)].

The magnetoresistivity $\rho(B)$ curves measured with the $B||c$ axis [Fig. 8(a)] reflect the field-induced magnetic transitions observed on the $M_c(B)$ curves. In this case we have clearly observed the increase of the resistivity at the lower-field metamagnetic transition, together with hysteresis comparable to that observed in the $M_c(B)$ curves. The fact that the a axis is the hard axis of the system is projected to the small

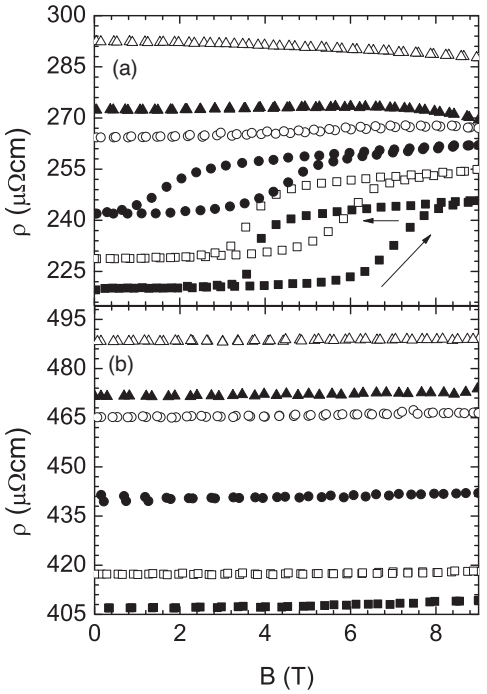

FIG. 8. The magnetoresistivity of the compound measured in the configuration (a) I || a axis, $B||c$ axis and (b) $I||c$ axis, $B||a$ axis. The temperatures of the experiment are as follows: (solid squares) 2 K; (open squares) 10 K; (solid circles) 15 K; (open circles) 20 K; (solid triangles) 25 K; (open triangles) 40 K.

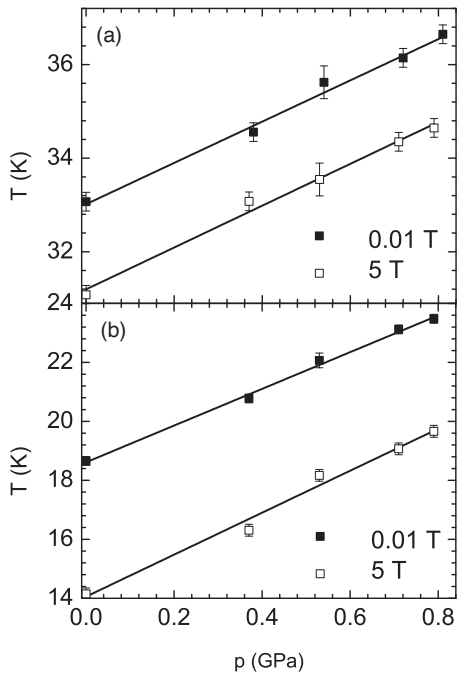

FIG. 9. The evolution of (a) T_N and (b) T_t with respect to the hydrostatic pressure. In all cases the transition temperatures were obtained from the ZFC-scan magnetization measurements in a magnetic field applied along the c axis. The lines represent the best linear fits as described in text.

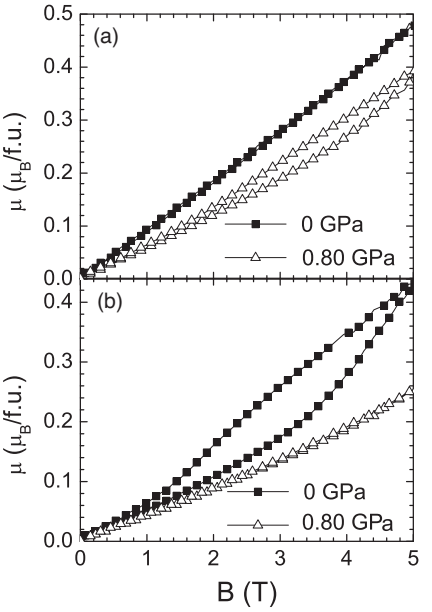

FIG. 10. The $M(B)$ curves measured at different hydrostatic pressures for the magnetic field applied along the c axis. The temperatures at which these measurements were performed were (a) 20 K and (b) 15 K.

increase of the magnetoresistivity due to Lorentz force for the configuration $B||a$ axis [Fig. 8(b)].

We are aware of the rather low residual resistivity ratio (RRR) values of our single crystals (3 for the a-axis and 2.4 for the c-axis data). The low RRR value originates from a high residual resistivity, which is generally mostly due the scattering on lattice defects. Since we know that the α and β phases differ in the stacking of the crystallographic basal-plane layers, one may suspect that the majority of the lattice defects in our case can be the stacking faults in the basal-plane sequence along the c axis. High-resolution transition electron microscopy investigations may help to resolve this issue by direct experiment. In antiferromagnets the residual resistivity may be partially enhanced due to Fermi surface nesting caused by the different magnetic and crystal structured periodicity, which is also our case.

Referring to the review article by Gignoux and Schmitt[15] we estimate that the leading exchange interaction in the α-$NdIr_2Si_2$ is the RKKY interaction. This interaction is oscillatory and long range, and that is why it depends crucially on the distance and position of the magnetic ions in the crystal. The hydrostatic pressure changes the distances between the magnetic ions and, hence, changes the RKKY interaction. This may lead to the change of the magnetic structure. The NdRhSn case can serve as a good example.[16] The question of what happens to the magnetic transitions in α-$NdIr_2Si_2$ if one applies the hydrostatic pressure (p) attracted our attention.

During our pressure experiment we measured the data only during heating after the previous cooling in the zero magnetic field. It means that we obtained no information about the hysteresis of T_t. Our pressure experiment up to 0.8 GPa revealed the linear increase of both T_N and T_t (Fig. 9). In the case of T_N, the increase is always 4.4(2) K GPa regardless

the applied magnetic field (up to $B = 5$ T). In the case of T_t, the slope of T_t versus p is only 6.2(2) K/GPa for a magnetic field of 0.01 T but as high as 7.1(3) K/GPa for the applied field of 5 T.

As concerns the study of the shift of the MT with applied hydrostatic pressure, the limitation of our SQUID apparatus (maximum field of 5 T) did not allow us to see the complete MT (Fig. 10). Nevertheless, the data are good enough to state that the magnetic transition does not shift to lower magnetic fields with applied hydrostatic pressure. The hysteresis in the minor hysteresis loop at 15 K [Fig. 10(b)] decreases with applied hydrostatic pressure. This may mean that the transition shifts to higher magnetic fields. In the case of 20 K $M(B)$ scans, another hysteresis loop begins to appear at elevated hydrostatic pressures [Fig. 10(a)]. This second loop is directly connected with the shifting of T_t to higher temperatures with applied hydrostatic pressure.

B. Neutron diffraction experiments

Our bulk-property experiments proved that the magnetic structure in α-$NdIr_2Si_2$ is not the same for the temperature regions $T < T_t$ and $T_t < T < T_N$, respectively, contrary to Welter *et al.*,[10] who reported only the simple AF1 structure. To resolve these contradictions, we performed a new NPD experiment on E6, and, additionally, we studied a α-$NdIr_2Si_2$ single crystal on the E1 triple axis neutron spectrometer.

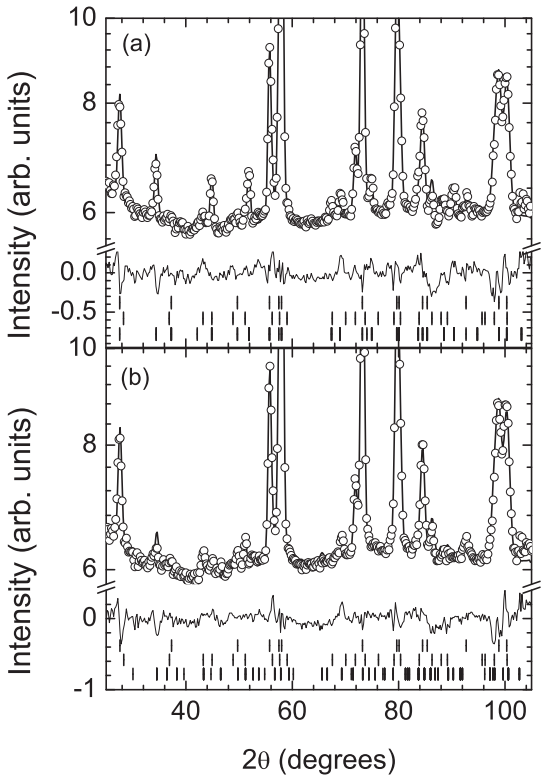

FIG. 11. (a) The refined pattern at $T = 2$ K; (b) the refined pattern at $T = 25$ K. In both cases we have plotted the observed data (circles), the calculated data (line behind the circles); the difference of the calculated and observed patterns (line below the circles), and the peak positions for (from up to down) the nuclear part of the α phase, the nuclear part of β phase, and the magnetic part of the α phase.

All the peaks in the NPD patterns collected at 2 K $< T < T_t$ [Fig. 11(a)] can be indexed by integer hkl indices for the tetragonal unit cell with the lattice parameters of the α phase plus the contribution from the paramagnetic impurity β phase. However, some of the peaks for the α phase appear at positions that are not consistent with the extinction rules for the $I4/mmm$ space group (basically: $h + k + l = 2n$; $n =$ integer), and they disappear at temperatures higher than T_t. Note that we have only 18% of the β phase in our sample. In the case where the β phase orders magnetically at temperatures higher than 2 K, the magnetic contribution from the β phase to the overall pattern is so low that we were unable to distinguish it from the background data. Taking into account the bulk magnetization measurements, we were able to index all peaks of the α phase using a simple antiferromagnetic structure with the magnetic propagation vector $\mathbf{k} = (0\ 0\ 1)$ and with the magnetic moments aligned along the c axis. We used this magnetic structure where magnetic moments are localized only on the Nd ions and the crystal structure from room temperature as a starting model for the Rietveld analysis. We found a perfect match between our experimental data and the model [Fig. 11(a)]. The fit converged to a magnetic moment of 3.27 μ_B/Nd, equal to the theoretical ordered magnetic moment for the free Nd^{3+} ion. In the temperature range 2 K $< T < T_t$, our results agree well with the results presented by Welter *et al.*[10] Heating the sample above T_t resulted in the disappearance of the low-temperature magnetic peaks and growth of new peaks at different 2θ positions [Fig. 11(b)]. All of these new peaks disappear in the $T = 40$ K pattern, indicating that these peaks are of the magnetic origin. We were unable to describe them by the integer hkl indices for the tetragonal unit cell, but their positions in 2θ are very close to the magnetic peaks observed for $T < T_t$ and so the assumption that the magnetic structure above T_t had a very similar propagation vector to the magnetic structure below T_t seemed reasonable. Following this assumption, we started the Rietveld analysis of the 25 K NPD pattern with the following model: the same nuclear structure as at $T = 300$ K, magnetic moments present only on the Nd ions, and moments locked along the c axis. As the starting value of the magnetic wave vector we used $\mathbf{k} = (0\ 0\ 0.9)$ and for the starting moment of the Nd ions we used 3.27 μ_B (theoretical magnetic moment for Nd^{3+} ion). The fit [Fig. 11(b)] converged to the magnetic wave vector $\mathbf{k} = [0\ 0\ 0.836(3)]$ and the magnetic moment 3.27(2) μ_B. This $\mathbf{k}$ vector is within experimental error equal to $\mathbf{k} = (0\ 0\ 5/6)$ and was not reported by Welter *et al.*[10]

To verify the magnetic structure obtained from the NPD experiment, and to determine the behavior under the applied magnetic field, we performed a single-crystal neutron diffraction experiment. During this experiment we investigated the (1 0 0), (1 0 2), and (2 0 1) magnetic reflections in the temperature range $2 < T < T_t$. The intensity of these reflections decreased with increasing temperature, and the reflections disappeared around T_t [Fig. 12(a)]. At temperatures $T_t < T < T_N$ we observed the (1 0 0.16(2)) = (1 0 1−q), (1 0 −0.16(2)) = (1 0 −1 + q), (1 0 1.83(2)) = (1 0 1+q),

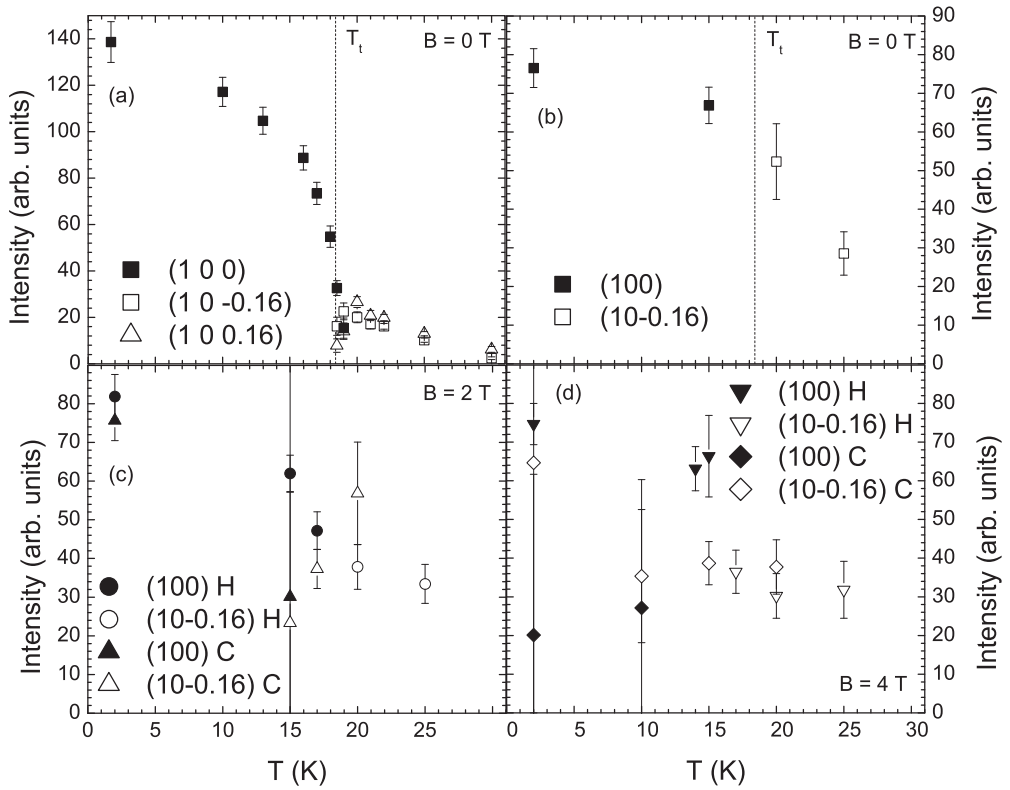

FIG. 12. Temperature evolution of the representative magnetic reflections. (a) Measured in Orange cryostat; [(b)–(d)] measured in HM1 magnet with applied field 0, 2, and 4 T. In all cases the magnetic field was applied at lowest temperature then we have measured during heating (H) the sample and cooling (C) the sample.

and despite of vicinity of the reflection from the aluminum holder, also the (2 0 1.17(2)) = (2 0 2−q); $q = 0.83(2)$ magnetic reflections [Fig. 12(a)]. At temperatures higher than 40 K, we observed only the nuclear reflections. These observations prove that the **k** vectors determined from our NPD experiment are correct. Within experimental error, we found no magnetic intensity in the hkl scans (0 0 0.75)-(0 0 1.25) and (0 0 2.7)-(0 0 3.1); this was a cross-check that all the magnetic moments are aligned along the c axis. Unfortunately, the precision of our measurement ($l = 0.02$) and the lower quality of our sample (due to β- to α-phase transition) prevented us from distinguishing if q is exactly 5/6 or slightly different. Based on the theoretical work of P. Bak[17] we decided that the magnetic structure with $q = 5/6$ is correct. We also studied in detail the region around the hkl position (1 0 1.5) = (1 0 −1 + 3q) at $T = 21$ K, but observed no magnetic signal. This suggests that the magnetic structure at temperatures $T_t < T < T_N$ is the normal longitudinal sine-modulated one.

Applying a magnetic field of 2 T and 4 T at 2 K left the (1 0 0) reflection unchanged [Figs. 12(b)–12(d)]. Increasing the temperature led to the decreasing intensity of this reflection, and at temperatures slightly lower that T_t, this reflection split into (1 0 0.16(2)) and (1 0 −0.16(2)). After heating the sample to 40 K, and during subsequent cooling in the applied magnetic field, a reversal process takes place at temperatures lower (hysteresis) than for the heating conditions. Note that in the case of 4 T, the reverse process was not complete even at 2 K, and the coexistence of all three magnetic peaks was observed. In the field scan at 15 K (Fig. 13), the change from the (1 0 0) reflection to the (1 0 0.16(2)) and (1 0 −0.16(2)) reflections and back was also observed with the hysteresis larger than 2 T.

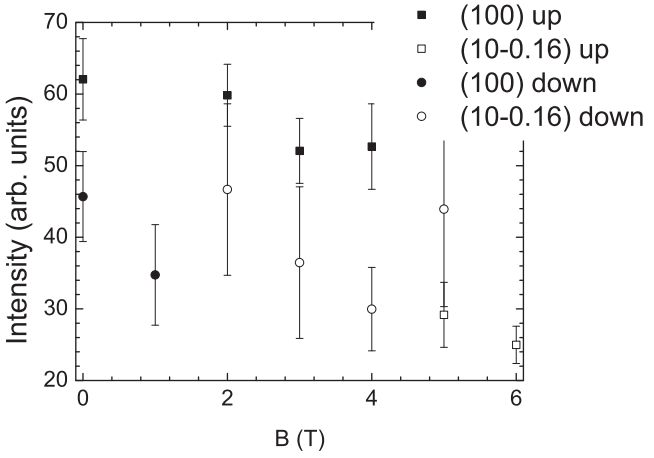

FIG. 13. Single-crystal neutron diffraction data for the field scan at $T = 15$ K. The full symbols represent the characteristic peaks for the AF1 phase; the opened symbols represent the characteristic peaks for the HF phase.

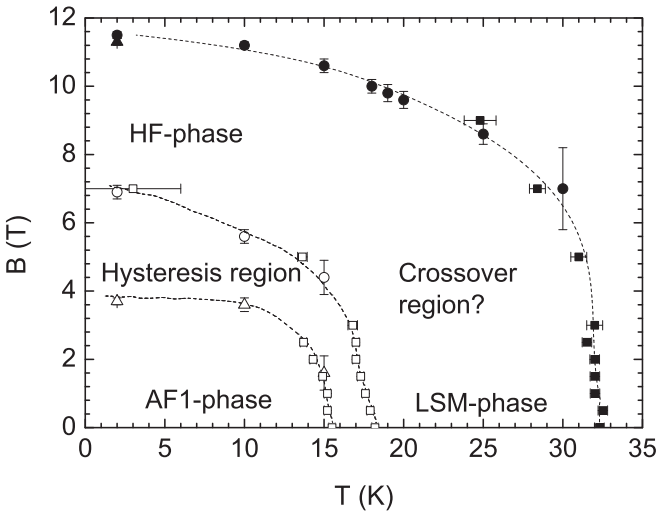

FIG. 14. The magnetic phase diagram for a magnetic field applied along the c axis showing evolution of the T_N (full symbols) and evolution of T_t (opened symbols). The points are derived from the anomalies in the magnetization observed on the temperature scans measured with the increasing temperature (squares), field scans during increasing the magnetic field (circles), and field scans during the decreasing of the magnetic field (triangles). The lines are guides for the eye.

C. Magnetic phase diagram

The presented data allow us to construct the magnetic phase diagram of α-$NdIr_2Si_2$. In a zero magnetic field two antiferromagnetic phases exist: the simple antiferromagnetic AF1-type phase (labeled as AF1 phase) at temperatures $T < 15.5(2)$ K and a longitudinal sine-modulated magnetic phase (LSM phase) with a propagation vector $\mathbf{k} = (0\ 0\ 5/6)$ at temperatures $18.2(2) < T < 32.3(3)$ K. In the temperature region $15.5(2) < T < 18.2$ K the compound can adopt either the AF1 phase or the LSM phase depending on the sample history. These phases remain intact in a magnetic field $B < 9$ T applied along the a axis. The phase diagram for the magnetic field applied along the c axis (Fig. 14) is richer. In this case we observed the phase transformation from AF1 phase to a different phase (HF phase), which is characterized by the spontaneous magnetic moment of 0.7 μ_B. A striking result is that this phase is (at least partially) characterized by the propagation vector $\mathbf{k} = (0\ 0\ 5/6)$: the magnetic propagation vector of the LSM phase at $B = 0$ and $T_t < T < T_N$. Naturally, one does not expect that the HF phase is equal to the LSM phase, but at this point we cannot exclude this possibility [for example the case of $PrCo_2Si_2$,[18,19] and HoAlGa (Ref. 20 and references therein)]. Note that we observed no peak/bump/kink anomalies in the bulk measurements (resistivity, magnetization, specific heat), which should point to the phase transformation from the HF phase to the LSM phase. A different, more feasible scenario is that HF phase consists of two $\mathbf{k}$ vectors: $\mathbf{k}_1 = (0\ 0\ 5/6)$ and $\mathbf{k}_2$ which can continuously emerge at very low magnetic fields, and we did not observe it in our high-field neutron experiment. The possibility of this scenario is based on our experimental constraints: the windows of HM1 magnet and the scattering plane defined by the (2 0 0) and (0 0 2) vectors. We can speculate if the small discrepancies between the ZFC, and FC curves in the temperature range $T_t < T < T_N$ (inset of Fig. 4) corroborate this scenario but, as we have no direct experimental data, this question remains open. In this case, there should be some sort of a crossover region between the HF phase and the LSM phase in the phase diagram (labeled "Crossover region' but with a question mark). To determine $\mathbf{k}_2$, a new neutron diffraction experiment is needed.

Further increasing the magnetic field leads to the phase transition at $B = 11.5(2)$ T. The high-field phase is characterized by a spontaneous moment of 2.9(1) μ_B, which is still considerably lower than the magnetic moment determined from the powder neutron diffraction. We cannot answer if the high-field magnetic structure is already a field-induced ferromagnetic state, and that the observed low magnetic moment is connected with the crystal field in the compound [as in α-$PrIr_2Si_2$ (Ref. 6)], or if other, different magnetic phases exist.

We have also observed a large hysteresis region in which the α-$NdIr_2Si_2$ can adopt two different magnetic phases (the AF1 phase or the HF phase) and the state of the studied compound depends on the history of the material. Our proposed phase diagram has similarities with the phase diagram of α-$PrIr_2Si_2$.[6] It differs only in the different T_t, T_N value of the critical magnetic field and, potentially, some additional magnetic phases at magnetic fields above 14 T.

IV. CONCLUSIONS

Although we failed to prepare pure β-$NdIr_2Si_2$ samples, we have proved that $NdIr_2Si_2$ belongs to the polymorphic family of compounds, which crystallize in the $CaBe_2Ge_2$, and $ThCr_2Si_2$ crystallographic modifications. Two different ordered magnetic phases are observed in α-$NdIr_2Si_2$: longitudinal sine-modulated with the magnetic propagation vector $\mathbf{k} = (0\ 0\ 5/6)$ in the temperature range $18.2(2)\ \text{K} < T < 32.3(3)$ K and simple antiferromagnetic AF1-type structure for $2\ \text{K} < T < 18.2(2)$ K. In both antiferromagnetic phases, we found magnetic moments only on the Nd ions. These moments are ordered along the c axis (easy-magnetization direction in the compound) and are equal to the theoretical prediction for the free Nd^{3+} ion. That is why we conclude the fully localized magnetism in this material.

Application of a magnetic field along the c axis destabilizes the AF1 phase and leads to the HF phase with the propagation vectors $\mathbf{k}_1 = (0\ 0\ 5{+}6)$ and probably $\mathbf{k}_2$, as yet unobserved. This transition is associated with an increase of electrical resistivity, which is consistent with the change of periodicity and the consequent change of nesting of the Fermi surface. This HF phase can be destabilized by a magnetic field of 11.5(2) T applied along the c axis. The application of the magnetic field along the a axis leads to no phase transitions in fields up to 9 T and confirms the strong uniaxial magnetocrystalline anisotropy of α-$NdIr_2Si_2$.

ACKNOWLEDGMENTS

The authors thank P. Henry for careful reading and correcting the manuscript. The work of V.S. is a part of the research plan MSM 0021620834 that is financed by the Ministry of Education of the Czech Republic. It was also supported by the Grant No. 202/09/1027 of the Czech Science Foundation.

*matus.mihalik@helmholtz-berlin.de

[1] H. F. Braun, N. Engel, and E. Parthé, Phys. Rev. B **28**, 1389 (1983).
[2] K. Hiebl, C. Horvath, and P. Rog, J. Less-Common Met. **117**, 375 (1986).
[3] D. Niepmann and R. Pöttgen, Intermet. **9**, 313 (2001).
[4] M. Mihalik, M. Diviš, and V. Sechovský, Physica B **404**, 3191 (2009).
[5] M. Mihalik, Z. Matěj, and V. Sechovský, Intermet. **17**, 927 (2009).
[6] M. Mihalik, M. Diviš, V. Sechovský, N. Kozlova, J. Freudenberger, N. Stüßer, and A. Hoser, Phys. Rev. B **81**, 174431 (2010).
[7] W. Zhong, B. Lloret, W. Ng, B. Chevalier, J. Etourneau, and P. Hagenmuller, Rev. Chim. Miner. **22**, 711 (1985).
[8] Z. Hossain, C. Geibel, F. Weickert, T. Radu, Y. Tokiwa, H. Jeevan, P. Gegenwart, and F. Steglich, Phys. Rev. B **72**, 094411 (2005).
[9] E. H. E. Ghadraoui, J. Y. Pivan, R. Guérin, O. P. amd J. Padiou, and M. Sergent, Mater. Res. Bull. **23**, 1345 (1988).
[10] R. Welter, K. Halich, and B. Malaman, J. Alloys Compd. **353**, 48 (2003).
[11] J. R.-Carvajal, Physica B **192**, 55 (1993).
[12] J. Christian, in *The Theory of Transformations in Metals and Alloys*, 3rd ed. (Elsevier Science Publishers, 2002), Vol. 1, Chap. 10, pp. 422–479.
[13] J. Kamarád, Z. Machátová, and Z. Arnold, Rev. Sci. Instrum. **75**, 5022 (2004).
[14] A. Eiling and J. S. Schilling, J. Phys. F **11**, 623 (1981).
[15] D. Gignoux and D. Schmitt, J. Magn. Magn. Mater. **100**, 99 (1991).
[16] M. Mihalik, J. Prokleška, J. Kamarád, K. Prokeš, O. Isnard, G. J. McIntyre, A. Dönni, S. Yoshii, H. Kitazawa, V. Sechovský, and F. R. de Boer, Phys. Rev. B **83**, 104403 (2011).
[17] P. Bak, Rep. Prog. Phys. **45**, 587 (1982).
[18] M. Motokawa, H. Nojiri, and Y. Endoh, Physica B **177**, 279 (1992).
[19] T. Kawae, M. Mito, M. Hitaka, F. Ichikawa, T. Shigeoka, N. Iwata, and K. Takeda, J. Phys. Soc. Jpn. **69**, 586 (2000).
[20] A. R. Ball, D. Gignoux, D. Schmitt, and F. Y. Zhang, Phys. Rev. B **47**, 11887 (1993).